

Addressing Sample Inefficiency in Multi-View Representation Learning

Kumar Krishna Agrawal^{1*} Arna Ghosh^{2*} Adam Oberman^{2,3} Blake Richards^{2,3,4,5}

¹ UC Berkeley ² Mila - Quebec AI Institute & McGill University
³ Canada CIFAR AI Chair ⁴ CIFAR Learning in Machines & Brains
⁵ Montreal Neurological Institute

Abstract

Non-contrastive self-supervised learning (NC-SSL) methods like BarlowTwins and VICReg have shown great promise for label-free representation learning in computer vision. Despite the apparent simplicity of these techniques, researchers must rely on several empirical heuristics to achieve competitive performance, most notably using high-dimensional projector heads and two augmentations of the same image. In this work, we provide theoretical insights on the implicit bias of the BarlowTwins and VICReg loss that can explain these heuristics and guide the development of more principled recommendations. Our first insight is that the orthogonality of the features is more critical than projector dimensionality for learning good representations. Based on this, we empirically demonstrate that low-dimensional projector heads are sufficient with appropriate regularization, contrary to the existing heuristic. Our second theoretical insight suggests that using multiple data augmentations better represents the desiderata of the SSL objective. Based on this, we demonstrate that leveraging more augmentations per sample improves representation quality and trainability. In particular, it improves optimization convergence, leading to better features emerging earlier in the training. Remarkably, we demonstrate that we can reduce the pretraining dataset size by up to 4x while maintaining accuracy and improving convergence simply by using more data augmentations. Combining these insights, we present practical pretraining recommendations that improve wall-clock time by 2x and improve performance on CIFAR-10/STL-10 datasets using a ResNet-50 backbone. Thus, this work provides a theoretical insight into NC-SSL and produces practical recommendations for enhancing its sample and compute efficiency.

1 Introduction

Unsupervised representation learning, i.e., learning features without human-annotated labels, is critical for progress in computer vision. Modern approaches, grouped under the *self-supervised learning (SSL)* umbrella, build on the core insight that *similar* images should map to nearby points in the learned feature space. Current SSL methods can be broadly categorized into contrastive and non-contrastive algorithms. While both categories aim to learn the desired features using “positive” samples, which refer to different augmentations of the same image, they diverge in using “negative” samples. Contrastive methods use augmentations obtained from entirely different images as negative samples to avoid the trivial solution of mapping all samples to the same point in the feature space (i.e., representational collapse). But, this necessitates an elaborate sampling scheme and huge batch sizes. Non-contrastive methods, on the other hand, eliminate the need for negative

*equal contribution

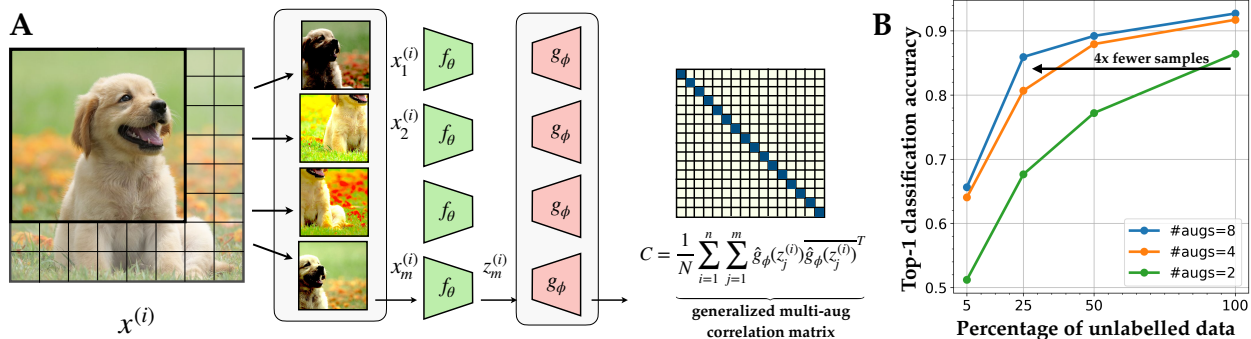


Figure 1: Design of existing SSL algorithms relies on heuristics. (A) We investigate the theoretical underpinnings of (i) the number of augmentations and (ii) the dimensionality of the projector g_ϕ . (B) We show that a generalized NC-SSL loss with multiple augmentations, & low-dimensional projectors outperforms existing heuristics while using $\sim 4\times$ smaller pretraining dataset.

samples altogether and instead rely on regularizing the feature space to avoid representational collapse.

A prominent subgroup among non-contrastive SSL methods is the family of Canonical Correlation Analysis (CCA) algorithms, which includes BarlowTwins [ZJM⁺21] and VICReg [BPL21]. These methods aim to enforce orthogonality among the learned features in addition to learning to map similar images to nearby points in feature space and have been shown to achieve competitive performance on benchmark computer vision datasets. These methods have become the preferred strategy for representation learning in several domains due to the lack of need for negative samples and their simple formulation. However, despite the apparent simplicity of their loss functions, the behavior of this family of algorithms is not well understood. Therefore, researchers often use empirically driven heuristics to design successful applications, such as using (i) a high-dimensional projector head or (ii) two augmentations per image. Although these heuristics help in practice, their theoretical underpinnings are unclear.

Alongside relying on heuristics and researchers’ intuition for design, existing SSL algorithms are extremely data-hungry. In particular, state-of-the-art algorithms often rely on large-scale datasets [RDS⁺15] or data engines [ODM⁺23] to achieve good representations. While this strategy works exceptionally well in natural-image settings, its application is limited in other critical domains, such as medical imaging, where the number of samples is scarce.

With these challenges in mind, the primary focus of this work is making progress toward establishing theoretical foundations underlying the family of non-contrastive SSL algorithms (NC-SSL) with an eye toward sample efficiency. In particular, we analyze the BarlowTwins and VICReg losses and show that they implicitly learn the data similarity kernel defined by the chosen augmentations. We show that learning the data similarity kernel is helped by greater orthogonality in the projector outputs and more data augmentations. As such, increasing the orthogonality of the projector output eliminates the requirement for a high-dimensional projector head, and increasing the number of data augmentations decreases the number of unique samples required. Our theoretical analysis establishes a principled grounding for the role of multiple augmentations and the sufficiency of low-dimensional projectors, outlining a framework for improving the sample efficiency of NC-SSL while maintaining representation quality.

We empirically verify our theoretical insights using the popular ResNet-50 backbone on benchmark datasets, CIFAR-10 and STL-10. Strikingly, we show that our multi-augmentation approach can learn good features even with a quarter of the samples in the pretraining dataset. As such, this suggests that SSL training can be done with smaller datasets and opens exciting questions in the design of performance-enhancing transformations. In summary, our core contributions are:

- **Eigenfunction interpretation:** We demonstrate that the loss functions of the CCA family of non-contrastive SSL algorithms are equivalent to the objective of learning eigenfunctions of the augmentation-defined data kernel.
- **Role of heuristics:** We provide a mechanistic explanation for the role of projector dimensionality and the number of data augmentations and empirically demonstrate that low-dimensional projector heads are sufficient and that using more augmentations leads to learning better representations.
- **Data efficient NC-SSL:** Leveraging the convergence benefits of the multi-augmentation framework, we demonstrate that we can learn good features with significantly smaller datasets (up to 25%) without harming downstream performance.

2 Related Work

Self-Supervised Pretraining requires significant compute resources, and with the lack of a unified theoretical framework, most practitioners rely on empirical heuristics. The SSL cookbook [BIS⁺23] provides a comprehensive summary of several widely adopted practices. While recent advances in SSL theory explore learning dynamics in linear (or shallow) models [TYCG20, TCG21], with a focus on understanding dimensionality collapse [JVLT21, GMAR22], the theoretical underpinnings of most “recipes” essential for good feature learning, are missing.

Contrastive SSL has received more theoretical attention, owing to its connection with metric learning and noise contrastive estimation [LPSG21, BL22, JHM23]. In particular, [HWGM21] provides a theoretical framework for the SimCLR loss from an augmentation graph perspective, which leads to practical recommendations. Subsequently, [GCB⁺22] establish a duality between contrastive and non-contrastive learning objectives, further bridging the gap between theory and practice.

Non-contrastive SSL algorithms have comparatively scarce theoretical foundations. In prior work [AMGR22, GCB⁺22] find that with modified learning objectives, low-dimensional projectors are sufficient for good downstream performance. Similarly, previous works have demonstrated notable performance boosts when using a multi-patch framework in contrastive [DAT⁺21] and non-contrastive SSL. However, the theoretical basis for the benefits and trade-offs of either low-dimensional projectors or multiple augmentations is unclear.

Deep Learning theory has made significant strides in understanding the optimization landscape and dynamics of supervised learning [ASS20]. In concurrent works, [ZLR⁺23, CKB⁺23] explore the interplay between the inductive bias of data augmentations, architectures, and generalization. In recent work, [SKZ⁺23] uses a more straightforward formulation of the BarlowTwins loss and investigates the learning dynamics in linearized models for the case when the invariance and orthogonalization losses have equal penalties.

3 Preliminaries

We start by formally defining the unsupervised representation learning problem for computer vision. In particular, we assume access to a dataset $\mathcal{D} = \{x_1, x_2, \dots, x_n\}$ with $x_i \in \mathbb{R}^p$ consisting of

unlabeled instances (often natural images), and the objective is to learn a d -dimensional representation ($d < p$) that is useful across multiple downstream applications. We focus on learning the parameters of a deep neural network $f_\theta \in \mathcal{F}_\Theta$, using the multi-view invariance SSL framework, wherein multiple views of an example are used to optimize pretraining loss function, $\mathcal{L}_{\text{pretrain}}(f_\theta, \mathcal{D})$

Non-Contrastive Self-Supervised Learning (NC-SSL) algorithms impose invariance to *data augmentations*, which are used to define multiple views of the same image while imposing specific regularization on the geometry of the learned feature space. More generally, both families can be thought of as decomposing $\mathcal{L}_{\text{pretrain}}$ into two terms (i) $\mathcal{L}_{\text{invariance}}$: to learn invariance to data augmentations and (ii) $\mathcal{L}_{\text{collapse}}$ to prevent collapsing the feature space to some trivial solution with no discriminative power.

$$\mathcal{L}_{\text{pretrain}} := \mathcal{L}_{\text{invariance}} + \beta \mathcal{L}_{\text{collapse}} \quad (1)$$

where β denotes a hyperparameter that controls the importance of the collapse-preventing term relative to the invariance term.

This formulation separates instance-level attributes invariant to augmentations, highlighting the semantic information of the instance. The ideal feature space is less sensitive to varying attributes and more sensitive to semantic ones, facilitating generalization to new examples. Understanding the interplay between pretraining loss and preserved attributes is critical for time and compute efficiency.

Data Augmentation graph was introduced by [HWGM21] to analyze contrastive losses, like SimCLR [CKNH20]. Briefly, we define a graph $\mathcal{G}(\mathcal{X}, \mathcal{W})$ with the vertex set (\mathcal{X}, ρ_X) comprising the result of all possible data augmentations from each sample in a dataset (could be infinite when continuous augmentation functions are used) and \mathcal{W} denoting the adjacency matrix. Let x_0 be an image in \mathcal{X} , and let $z = M(x_0)$ be a random data augmentation of the image, x_0 . We define the probability density of reaching z from x_0 via a choice of mapping M :

$$p(z | x_0) = \mathbb{P}(z = M(x_0)), \quad (2)$$

Since mapping is not generally invertible (e.g., crops), observe that $p(x_0 | z) \neq p(z | x_0)$. Using this definition, we now define the strength of the edge between nodes x and z of the augmentation graph as the joint probability of generating augmentations x, z from the same image $x_0 \sim \rho_X$. Formally,

$$w_{xz} := \mathbb{E}_{x_0 \sim \rho_X} [p(x | x_0)p(z | x_0)] \quad (3)$$

It is worth noting that the magnitude of w_{xz} captures the relative similarity between x and z . A higher value of w_{xz} indicates that both patches are more likely to come from the same image and, thereby, more similar.

[HWGM21] showed that optimizing a functionally equivalent form of the SimCLR loss termed the spectral contrastive loss (\mathcal{L}_c , essentially learns features whose covariance structure matches the adjacency matrix of the augmentation graph.

$$\mathcal{L}_c \propto \|ZZ^T - \bar{\mathcal{W}}\|_F^2 \quad (4)$$

where Z denotes the output of the neural network, $\bar{\mathcal{W}}$ denotes the degree-normalized adjacency matrix and $\|\cdot\|_F$ denotes the Frobenius norm operator. This perspective implies that the features learned by a contrastive SSL framework would align with the top eigenvectors of $\bar{\mathcal{W}}$. As observed by [HWGM21], all rotations of Z that don't change its span define an equivalence class of solutions to the above optimization problem and make no difference for the downstream generalization of a linear probe. Based on this insight, we define a notion of equivalence among learned feature spaces.

Definition 3.1. Let $F(x) = (f_1(x), \dots, f_d(x))$ be a d -dimensional feature vector (a vector of functions). Define the subspace

$$V = V(F) = \{h : X \rightarrow \mathbb{R} \mid h(x) = w \cdot F(x), \quad w \in \mathbb{R}^d\} \quad (5)$$

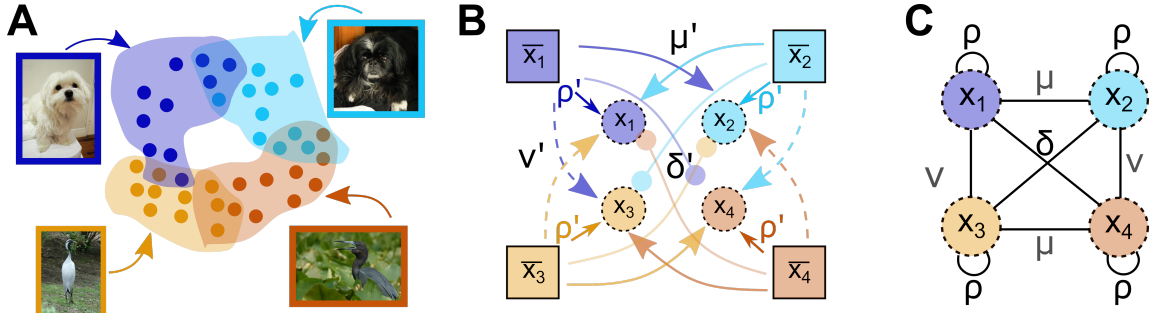


Figure 2: Schematic of augmentation graph. (A) Augmentations from each image span a region in the image space, which could overlap with the augmentation span of other images. (B) An augmentation graph schematic that uses probabilities to characterize the interactions among augmentation spans of different instances.

to be the span of the components of F . Given an n -dimensional feature vector, $G(x) = (g_1(x), \dots, g_n(x))$ we say the features G and F are equivalent, if $V(F) = V(G)$.

4 Data augmentation kernel perspective of non-contrastive SSL

Following the previous section, we present an augmentation kernel perspective of BarlowTwins and VICReg losses. Specifically, we show that these losses are equivalent to the optimization problem of learning eigenfunctions of the augmentation-defined data covariance kernel. Subsequently, we argue that using a high-dimensional projector yields better overlap with the top eigenvectors of the data augmentation kernel at initialization compared to a low-dimensional projector. Therefore, our analysis suggests using a stronger orthogonalization constraint during optimization for lower-dimensional projectors to ensure that features learned are equivalent to those learned with high-dimensional projectors. Furthermore, we argue that using more augmentations improves our estimate of the augmentation-defined data covariance kernel, thereby aiding the eigenfunction optimization problem. Therefore, our analysis suggests using an averaging operator with more data augmentations to estimate the true augmentation kernel better.

4.1 Features in terms of data augmentation kernels

We will define two notions of the data augmentation kernel. Given two images, x, z , the first kernel, which we call the forward data augmentation covariance kernel, is given by

$$k^{DAF}(x, z) = \mathbb{E}_{x_0 \sim \rho_x} \left[\frac{p(x | x_0) p(z | x_0)}{\rho(x) \rho(z)} \right] \quad (6)$$

This covariance kernel measures the similarity between x, z in terms of how likely they are to be reached from x_0 , weighted by the distribution of x_0 . Note that this is the edge strength between nodes x, z in the augmentation graph. We can also define a (backward) data augmentation covariance kernel that reverses the roles of (x, z) and x_0 :

$$k^{DAB}(x, z) = \mathbb{E}_{x_0 \sim \rho_x} \left[\frac{p(x_0 | x) p(x_0 | z)}{\rho(x_0) \rho(x_0)} \right] \quad (7)$$

SSL aims to learn features that preserve the covariance kernel structure (imposed by this choice of mapping M) [DEHL22]. Therefore, we want to define a loss which determines *vector features*,

$F : X \rightarrow \mathbb{R}^d$, which factor a data augmentation kernel $k^{DA}(x, z) = F(x)^\top F(z)$. Doing this directly is prohibitively data-intensive at scale since it involves a search over data-augmented images. However, since the covariance kernels are PSD, they define a Reproducing Kernel Hilbert space (RKHS). This allows us to apply Mercer’s theorem to find vector features as in [DSZ⁺22a, DSZ22b, PPA⁺18].

The construction of features using Mercer’s theorem goes as follows. Given a PSD data augmentation kernel, k^{DA} , define the T_k operator, which takes a function f and returns its convolution with the data augmentation kernel.

$$T_k f(x) = \mathbb{E}_{z \sim \rho_X} [k(z, x) f(z)] \quad (8)$$

We will also make use of the following operator,

$$T_M f(x) = \mathbb{E}_{x_0 \sim M(x)} [f(x_0)] = \sum_{x_0} [p(x_0 | x) f(x_0)] \quad (9)$$

which averages the values of the function, f , over the augmented images $x_0 = M(x)$ of the data, x .

Since the operator T_k is compact and positive, it has a spectral decomposition consisting of eigenfunctions ϕ_i and corresponding eigenvalues λ_i . Using these eigenpairs, we can define the (infinite sequence of square summable) spectral features, $G : X \rightarrow \ell_2$, (where ℓ_2 represents square summable sequences), by

$$G(x) = (\sqrt{\lambda_1} \phi_1(x), \dots, \sqrt{\lambda_d} \phi_d(x), \dots) \quad (10)$$

Then, Mercer’s theorem gives

$$k^{DA}(x, z) = G(x) \cdot G(z) \quad (\text{Mercer})$$

and ensures that the inner product is finite. These are the desired features that factor in the kernel. However, computing the eigenfunctions of T_k is costly. Instead, we propose an alternative using the more efficient operator T_M . According to Definition 3.1, both operators lead to equivalent features.

Theorem 4.1. *Let $G(x)$ be the infinite Mercer features of the backward data augmentation covariance kernels, k^{DAB} . Let $F(x) = (f_1(x), f_2(x), \dots, f_k(x))$ be the features given by minimizing the following data augmentation invariance loss*

$$L(F) = \sum_{i=1}^{N_k} \|T_M f_i - f_i\|_{L^2(\rho_X)}^2, \quad \text{subject to} \quad (f_i, f_j)_{\rho_X} = \delta_{ij} \quad (11)$$

which includes the orthogonality constraint. Then, $V(F) \subset V(G)$, $V(F) \rightarrow V(G)$ as $N_k \rightarrow \infty$.

The idea of the proof uses the fact that, as linear operators, $T_{k^{DAB}} = T_M^\top T_M$ and that $T_{k^{DAF}} = T_M T_M^\top$. Then we use the spectral theory of compact operators, which is analog of the Singular Value Decomposition in Hilbert Space, to show that eigenfunctions of $T_M^\top T_M$ operator are the same as those obtained from optimizing $L(F)$. A similar result can be obtained using k^{DAF} and T_M^\top .

Note that $L(F)$ is the constrained optimization formulation of the BarlowTwins loss. Furthermore, $L(F)$ with the additional constraint that $(f_i, f_i) \geq \gamma \forall i \in \{1, 2 \dots N_k\}$ is the constrained optimization formulation of the VICReg loss.

4.2 Corollary 1: Low-dimensional projectors are sufficient

While BarlowTwins and VICReg frameworks have advocated using high-dimensional projectors to facilitate good feature learning on Imagenet, our kernel perspective challenges this notion. Since the intrinsic dimensionality of Imagenet is estimated to be ~ 40 [PZA⁺20], it is not unreasonable to expect that the span of desired features would be of similar dimensionality. It is, thus, intriguing

that these frameworks mandate the use of an $\sim 8192 - d$ projector head to capture the intricacies of the corresponding data augmentation kernel. This discrepancy can be explained by observing the learning dynamics of a linearized model under the BarlowTwins loss optimization [SKZ⁺23]. These dynamics reveal that initializing the projection weight matrix in alignment with the eigenfunctions of the data kernel retains this alignment throughout the learning process. Notably, a high-dimensional projector is more likely to have a greater initialization span than its low-dimensional counterpart, increasing the likelihood of overlap with the relevant eigenfunctions. We hypothesize that it is possible to rectify this issue by using a stronger orthogonalization constraint for low-dimensional projectors, thereby rendering them sufficient for good feature learning.

4.3 Corollary 2: Multiple augmentations improve optimization

Theorem 4.1 implies that the invariance loss optimization would ideally entail using the T_M operator, thereby requiring many augmentations for each sample x . Using only two augmentations per sample yields a noisy estimate of T_M , yielding spurious eigenpairs [Ver10] (see Appendix). These spurious eigenpairs add stochasticity to the learning dynamics and hinder the alignment of the learned features with the eigenfunctions of the data kernel [SKZ⁺23]. We hypothesize that improving this estimation error by increasing the number of augmentations could alleviate this issue and improve the speed and quality of feature learning.

Increasing the number of augmentations (say m) in BarlowTwins and VICReg comes with added compute costs. A straightforward approach would involve calculating the invariance loss for every pair of augmentations, resulting in $\mathcal{O}(m^2)$ operations. However, Theorem 4.1 proposes an alternative method that uses the sample estimate of T_M , thereby requiring only $\mathcal{O}(m)$ operations. Both these strategies are functionally equivalent (see Appendix), but the latter is computationally more efficient. In summary, Theorem 4.1 establishes a mechanistic role for the number of data augmentations, paving the way for a computationally efficient multi-augmentation framework:

$$\widehat{L}(F) = \mathbb{E}_{x \sim \rho_X} \left[\sum_{i=1}^{N_k} \sum_{j=1}^m \| \overline{f_i(x)} - f_i(x_j) \|_{L^2(\rho_X)}^2 \right], \quad \text{subject to} \quad (f_i, f_j)_{\rho_X} = \delta_{ij} \quad (12)$$

where $\overline{f_i(x)} = \frac{1}{m} \sum_{j=1}^m f_i(x_j)$ is the sample estimate of $T_M f_i(x)$.

5 Experiments

In our experiments, we seek to serve two purposes: (i) provide empirical support for our theoretical insights and (ii) present practical primitives for designing efficient self-supervised learning routines. In summary, with extensive experiments across learning algorithms (BarlowTwins, VICReg) and training datasets (CIFAR-10/STL-10), we establish that

- **low-dimensional projectors** as sufficient for learning *good representations*.
- **multi-augmentation** improves downstream accuracy and convergence.
- multi-Augmentation **improves sample efficiency** in SSL pretraining, i.e., recovering similar performance with significantly fewer unlabelled samples.

Experiment Setup: We evaluate the effectiveness of different pretraining approaches for non-contrastive SSL algorithms using image classification as the downstream task. Across all experiments, we use linear probing with Resnet-50 as the feature encoder backbone. On CIFAR-10, all models are

pretrained for 100 epochs, while STL-10 models are pretrained for 50 epochs. All runs are averaged over 3 seeds; error bars indicate standard deviation. Other details related to optimizers, learning rate, etc., are presented in the Appendix.

5.1 Sufficiency of Low-dimensional projectors

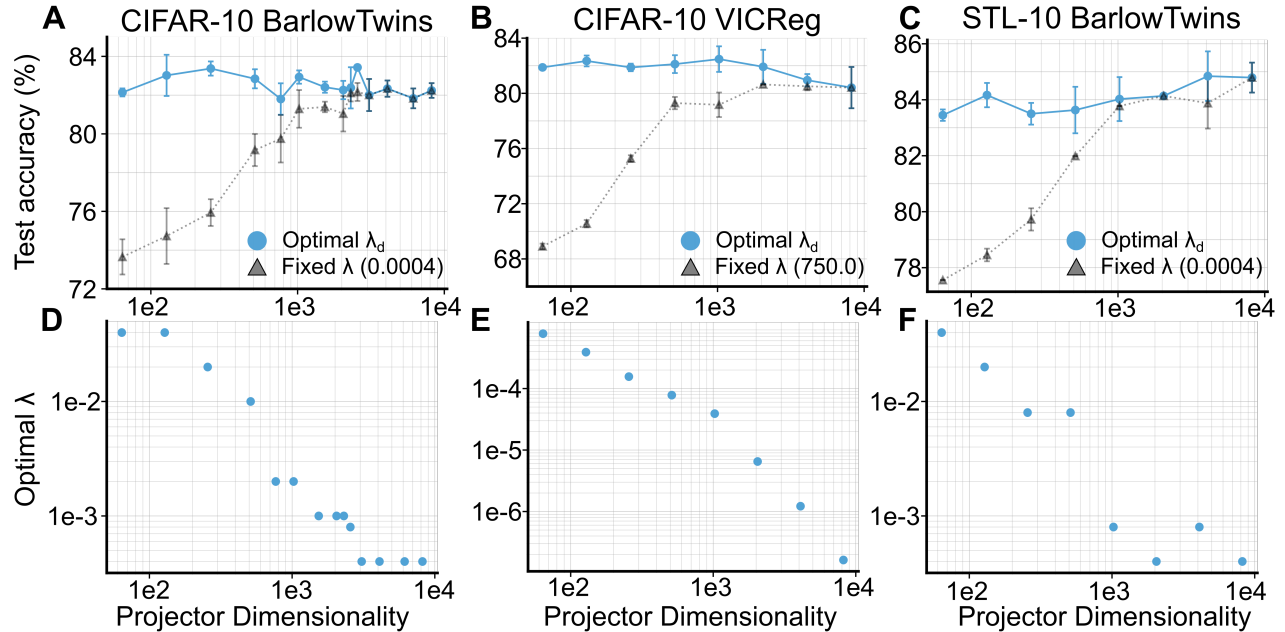


Figure 3: Low-dimensional projectors are sufficient for good feature learning. We demonstrate that using a higher orthogonality constraint (λ for D, F and $\lambda_{eff} = \frac{1}{d\lambda}$ for E) for lower projector dimensionality can achieve similar performance over a wide range of projector dimensions (d).

Existing works recommend using high-dimensional MLPs as projectors (e.g., $d=8192$ for Imagenet in [ZJM⁺21, BPL21]), and show significant degradation in performance for a fixed redundancy coefficient (λ). To reproduce this result, we run a grid search to find the optimal coefficient (λ_{8192}^*) for $d = 8192$ and show that performance progressively degrades for lower d if the same coefficient λ_{8192}^* is reused for $d \in \{64, 128, 256, 512, 1024, 2048, 4096, 8192\}$.

Our insights in Section 4.2 suggest low-dimensional projectors should recover similar performance with appropriate orthogonalization. To test this, we find the best λ by performing a grid search independently for each $d \in \{64, 128, 256, 512, 1024, 2048, 4096, 8192\}$. Low-dimensional projectors are sufficient, as illustrated in Figure 3. Strikingly, we also observe that the optimal $\lambda_d \propto 1/d$ is in alignment with our theoretical insights.

Recommendations: Start with low-dimensional projector, using $\lambda = \mathcal{O}(\frac{1}{d})$, and sweep over ($pdim = d, \lambda = \mathcal{O}(\frac{1}{d})$) if needed.

5.2 Multiple Augmentations Improve Performance and Convergence

Although some SSL pretraining approaches, like SWaV, incorporate more than two views, the most widely used heuristic in non-contrastive SSL algorithms involves using two views jointly

encoded by a shared backbone. In line with this observation, our baselines for examining the role of multiple augmentations use two views for computing the cross-correlation matrix.

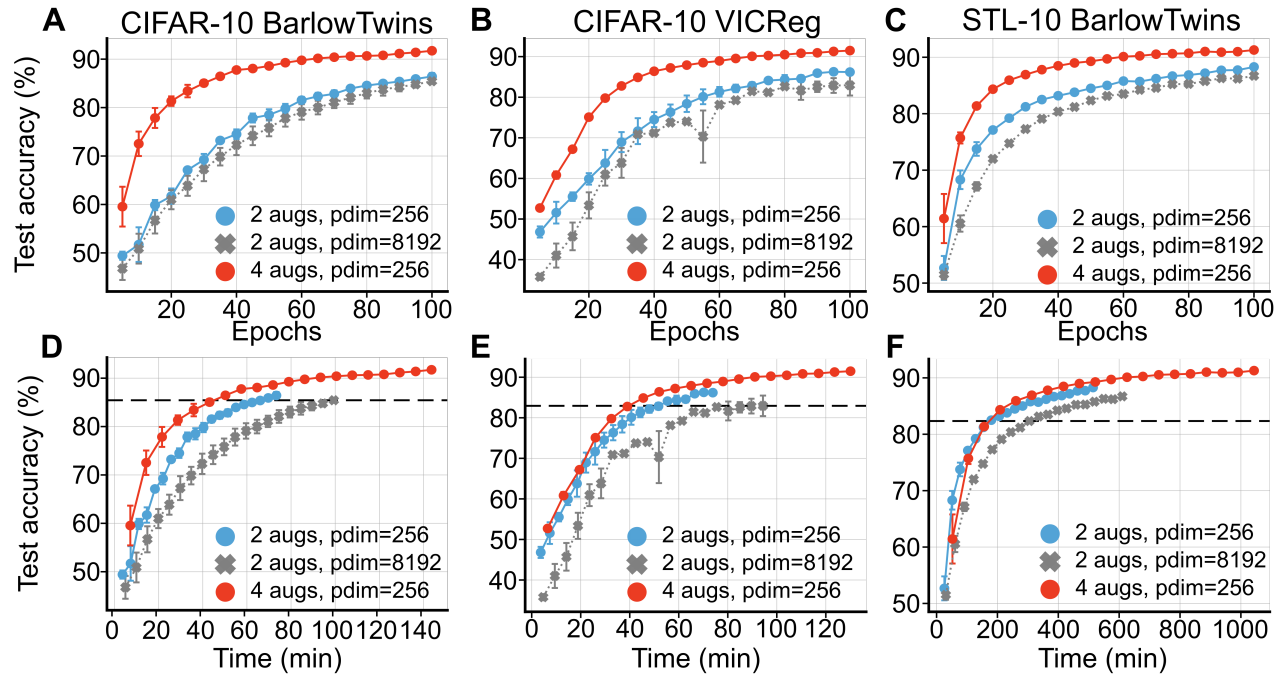


Figure 4: Using multiple augmentations improves representation learning performance and convergence. (A-C) Across BarlowTwins and VICReg for CIFAR-10 and STL-10 pretraining, using 4 augmentations instead of 2 helps improve performance. (D-F) Although the 4-augmentations take longer for each epoch, its performance still trumps the 2-augmentation version of the algorithm at the same wall clock time.

To understand the role of multiple augmentations in pretraining in light of the augmentation-kernel interpretation, we propose Equation (12), which generalizes Barlow-Twins and VICReg to the multi-augmentation setting. In particular, for $\#aug \in \{2, 4, 8\}$, we pretrain Resnet-50 with the generalized NC-SSL loss for 100 epochs on CIFAR-10 and 50-epochs for STL-10. Building on the insight from the previous section, we use a 256-dimensional projector head for all experiments.

In Figure 4, we track the downstream performance of the pre-trained models across training epochs, i.e., we extract features from intermediate checkpoints and train a linear classifier on top of the features. Here, we use the linear evaluation protocol as outlined by [CBL22]. Figure 4(A-C) shows that pretraining with multiple augmentations outperforms the 2-augmentation baseline. Furthermore, we observe that the four-augmentation pre-trained models converge faster (both in terms of the number of epochs and wall-clock time) than their two-augmentation counterparts (see Figure 4(D-F)).

Recommendation: Using multiple augmentations (> 2) with the generalized NC-SSL loss is likely to improve convergence as well as downstream accuracy.

5.3 Sample Efficient Multi-View Learning

Data Augmentation can be viewed as a form of data inflation, where the number of training samples is increased by k (for k augmentations). In this section, we examine the role of multi-augmentation in improving sample efficiency. In particular, we are interested in understanding if the same performance can be achieved with a fraction of the pretraining dataset.

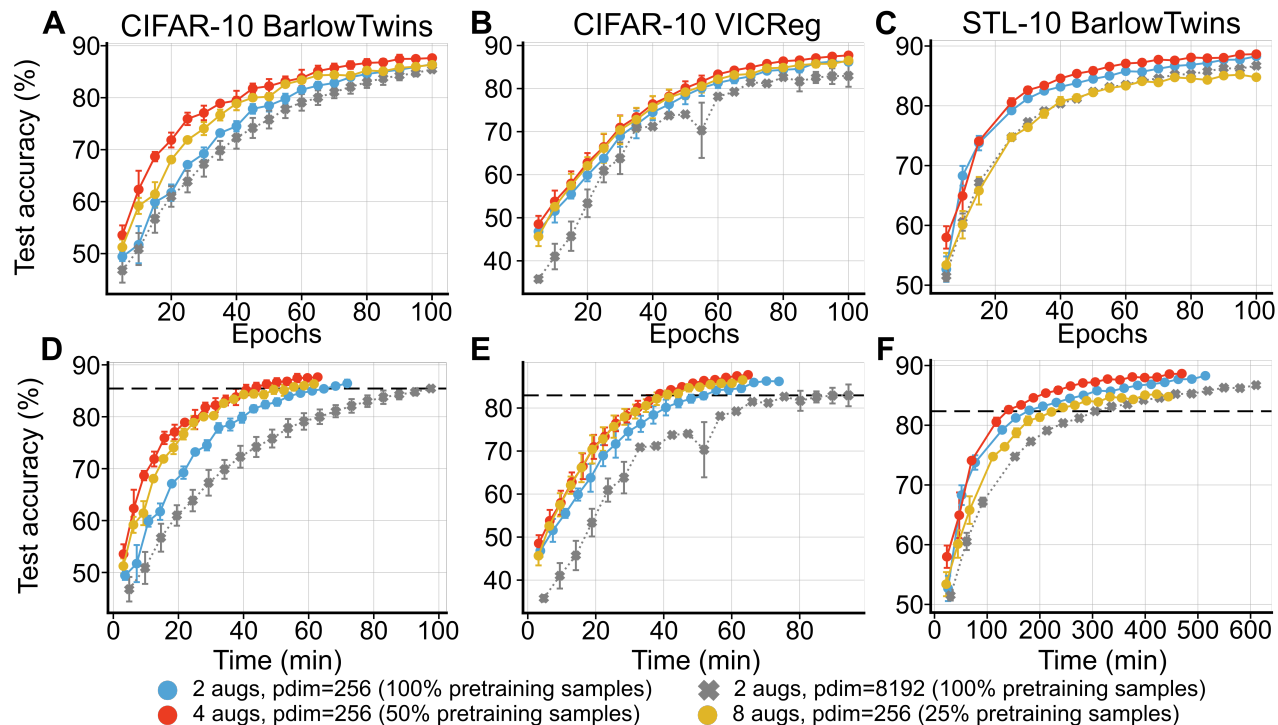


Figure 5: Multi-augmentation improves sample efficiency, recovering similar performance with significantly fewer unique samples in the pretraining dataset. Across BarlowTwins and VICReg pretraining on CIFAR-10 and STL-10, for the same effective dataset size ($\#aug \times \#unique_samples$), using more patches improves performance at the same epoch (A-C) or wall clock time (D-F). However, a tradeoff exists wherein doing more data augmentations fails to improve performance in the scarce data regime.

To examine the relation between the number of augmentations and sample efficiency, we fixed the effective size of the inflated dataset. This is achieved by varying the fraction of the unique samples in the pretraining dataset depending on the number of augmentations $k \in \{2, 4, 8\}$, e.g., we use 1/2 the dataset for 4 views. We then evaluate the performance of the pre-trained models on the downstream task, where the linear classifier is trained on the same set of labeled samples. Strikingly, Figure 5 shows that using multiple augmentations can achieve similar (sometimes even better) performance with lesser pretraining samples, thereby indicating that more data augmentations can be used to compensate for smaller pretraining datasets.

Recommendation: In a low-data regime, using diverse & multiple augmentations can be as effective as acquiring more unique samples.

6 Discussion

Summary: Our work presents a fresh theoretical analysis that sheds light on the implicit bias of non-contrastive SSL algorithms. We use these insights to unravel the impact of crucial design heuristics and offer practical recommendations that improve convergence while maintaining accuracy (on CIFAR-10/STL-10). We also show that the multi-augmentation framework can be used to learn good features from fewer unique samples in the pretraining dataset simply by improving the estimation of the data augmentation kernel.

Pareto Optimal SSL In the context of sample efficiency, training a model using two augmentations with different fractions of the dataset leads to a natural Pareto frontier, i.e., training on the full dataset achieves the best error but takes the most time (**Baseline (2-Aug)**). Our extensive experiments demonstrate that using more than two augmentations improves the overall Pareto frontier, i.e., achieves better convergence while maintaining accuracy (**Multi-Aug**). Strikingly, as shown in Figure 6, we observe that we can either use a larger pretraining dataset or more augmentations for a target error level. Therefore, the number of augmentations can be used as a knob to control the sample efficiency of the pretraining routine.

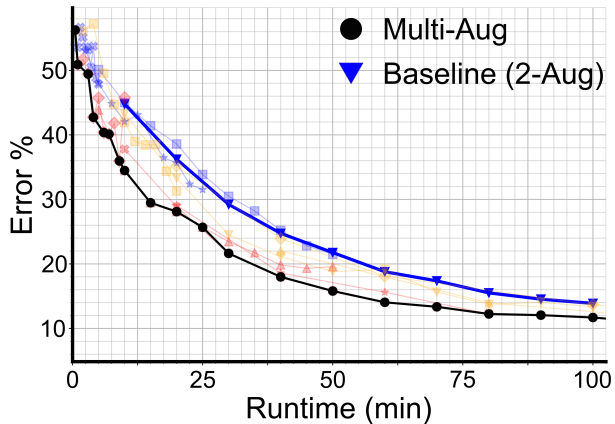


Figure 6: Using > 2 augmentations with a fraction of the dataset improves overall Pareto frontier, speeding runtime up to $\sim 2\times$.

Open Questions: Looking ahead, it would be exciting to extend this analysis to other categories of SSL algorithms, such as Masked AutoEncoders (MAE). Furthermore, our insights provide opportunities to explore sample-efficient methods that rely on less data, which is particularly important in critical domains such as medical imaging, where data is often scarce and expensive.

Limitations Our algorithm relies on multiple views of the same image to improve the estimation of the data-augmentation kernel. Although this approach does add some extra computational overhead, it significantly speeds up the learning process. We can explore the possibility of making the current design more computationally efficient to improve it further.

Acknowledgements

The authors would like to thank Arnab Kumar Mondal for insightful discussions that helped shape the project’s scope and Colleen Gillon for her aesthetic contribution to the figures. This research was generously supported by Vanier Canada Graduate Scholarship (A.G.); NSERC (Discovery Grant: RGPIN-2020-05105; Discovery Accelerator Supplement: RGPAS-2020-00031; Arthur B. McDonald Fellowship: 566355-2022) and CIFAR Learning in Machines and Brains Program (B.A.R.); Canada CIFAR AI Chair program (A.O. & B.A.R.). The authors also acknowledge the material support of NVIDIA in the form of computational resources.

References

- [AMGR22] Kumar K Agrawal, Arnab Kumar Mondal, Arna Ghosh, and Blake Richards. α -req: Assessing representation quality in self-supervised learning by measuring eigenspectrum decay. *Advances in Neural Information Processing Systems*, 35:17626–17638, 2022.
- [ASS20] Madhu S Advani, Andrew M Saxe, and Haim Sompolinsky. High-dimensional dynamics of generalization error in neural networks. *Neural Networks*, 132:428–446, 2020.
- [BIS⁺23] Randall Balestriero, Mark Ibrahim, Vlad Sobal, Ari Morcos, Shashank Shekhar, Tom Goldstein, Florian Bordes, Adrien Bardes, Gregoire Mialon, Yuandong Tian, et al. A cookbook of self-supervised learning. *arXiv preprint arXiv:2304.12210*, 2023.
- [BL22] Randall Balestriero and Yann LeCun. Contrastive and non-contrastive self-supervised learning recover global and local spectral embedding methods. In *NeurIPS*, 2022.
- [BPL21] Adrien Bardes, Jean Ponce, and Yann LeCun. Vicreg: Variance-invariance-covariance regularization for self-supervised learning. *arXiv preprint arXiv:2105.04906*, 2021.
- [CBLL22] Yubei Chen, Adrien Bardes, Zengyi Li, and Yann LeCun. Intra-instance vicreg: Bag of self-supervised image patch embedding. *arXiv preprint arXiv:2206.08954*, 2022.
- [CKB⁺23] Vivien Cabannes, Bobak Kiani, Randall Balestriero, Yann LeCun, and Alberto Bietti. The ssl interplay: Augmentations, inductive bias, and generalization. In *International Conference on Machine Learning*, pages 3252–3298. PMLR, 2023.
- [CKNH20] Ting Chen, Simon Kornblith, Mohammad Norouzi, and Geoffrey Hinton. A simple framework for contrastive learning of visual representations. In *International conference on machine learning*, pages 1597–1607. PMLR, 2020.
- [CNL11] Adam Coates, Andrew Y Ng, and Honglak Lee. An analysis of single-layer networks in unsupervised feature learning. In *International Conference on Artificial Intelligence and Statistics*, pages 215–223, 2011.
- [DAT⁺21] Debidatta Dwivedi, Yusuf Aytar, Jonathan Tompson, Pierre Sermanet, and Andrew Zisserman. With a little help from my friends: Nearest-neighbor contrastive learning of visual representations. In *Proceedings of the IEEE/CVF International Conference on Computer Vision*, pages 9588–9597, 2021.
- [DEHL22] Yann Dubois, Stefano Ermon, Tatsunori B Hashimoto, and Percy S Liang. Improving self-supervised learning by characterizing idealized representations. *Advances in Neural Information Processing Systems*, 35:11279–11296, 2022.
- [DSZ⁺22a] Zhijie Deng, Jiaxin Shi, Hao Zhang, Peng Cui, Cewu Lu, and Jun Zhu. Neural eigenfunctions are structured representation learners. *arXiv preprint arXiv:2210.12637*, 2022.
- [DSZ22b] Zhijie Deng, Jiaxin Shi, and Jun Zhu. Neuraief: Deconstructing kernels by deep neural networks. In *International Conference on Machine Learning*, pages 4976–4992. PMLR, 2022.
- [GCB⁺22] Quentin Garrido, Yubei Chen, Adrien Bardes, Laurent Najman, and Yann Lecun. On the duality between contrastive and non-contrastive self-supervised learning. *arXiv preprint arXiv:2206.02574*, 2022.

- [GMAR22] Arna Ghosh, Arnab Kumar Mondal, Kumar Krishna Agrawal, and Blake Richards. Investigating power laws in deep representation learning. *arXiv preprint arXiv:2202.05808*, 2022.
- [Goh90] I Gohberg. Classes of linear operator theory. *Advances and Applications*, 49, 1990.
- [HK12] Lajos Horváth and Piotr Kokoszka. *Inference for functional data with applications*, volume 200. Springer Science & Business Media, 2012.
- [HWGM21] Jeff Z HaoChen, Colin Wei, Adrien Gaidon, and Tengyu Ma. Provable guarantees for self-supervised deep learning with spectral contrastive loss. *Advances in Neural Information Processing Systems*, 34:5000–5011, 2021.
- [JHM23] Daniel D. Johnson, Ayoub El Hanchi, and Chris J. Maddison. Contrastive learning can find an optimal basis for approximately view-invariant functions. In *The Eleventh International Conference on Learning Representations, ICLR 2023, Kigali, Rwanda, May 1-5, 2023*. OpenReview.net, 2023.
- [JVL21] Li Jing, Pascal Vincent, Yann LeCun, and Yuandong Tian. Understanding dimensional collapse in contrastive self-supervised learning. *arXiv preprint arXiv:2110.09348*, 2021.
- [KH09] Alex Krizhevsky and Geoffrey Hinton. Learning multiple layers of features from tiny images. *Technical Report*, 2009.
- [LPSG21] Yazhe Li, Roman Pogodin, Danica J Sutherland, and Arthur Gretton. Self-supervised learning with kernel dependence maximization. *Advances in Neural Information Processing Systems*, 34:15543–15556, 2021.
- [ODM⁺23] Maxime Oquab, Timothée Darcet, Théo Moutakanni, Huy Vo, Marc Szafraniec, Vasil Khalidov, Pierre Fernandez, Daniel Haziza, Francisco Massa, Alaaeldin El-Nouby, et al. Dinov2: Learning robust visual features without supervision. *arXiv preprint arXiv:2304.07193*, 2023.
- [PPA⁺18] David Pfau, Stig Petersen, Ashish Agarwal, David GT Barrett, and Kimberly L Stachenfeld. Spectral inference networks: Unifying deep and spectral learning. *arXiv preprint arXiv:1806.02215*, 2018.
- [PZA⁺20] Phil Pope, Chen Zhu, Ahmed Abdelkader, Micah Goldblum, and Tom Goldstein. The intrinsic dimension of images and its impact on learning. In *International Conference on Learning Representations*, 2020.
- [RDS⁺15] Olga Russakovsky, Jia Deng, Hao Su, Jonathan Krause, Sanjeev Satheesh, Sean Ma, Zhiheng Huang, Andrej Karpathy, Aditya Khosla, Michael Bernstein, et al. Imagenet large scale visual recognition challenge. *International journal of computer vision*, 115:211–252, 2015.
- [SJK⁺22] Kendrick Shen, Robbie Jones, Ananya Kumar, Sang Michael Xie, Jeff Z HaoChen, Tengyu Ma, and Percy Liang. Connect, not collapse: Explaining contrastive learning for unsupervised domain adaptation. *arXiv preprint arXiv:2204.00570*, 2022.
- [SKZ⁺23] James B Simon, Maksis Knutins, Liu Ziyin, Daniel Geisz, Abraham J Fetterman, and Joshua Albrecht. On the stepwise nature of self-supervised learning. *arXiv preprint arXiv:2303.15438*, 2023.

- [TCG21] Yuandong Tian, Xinlei Chen, and Surya Ganguli. Understanding self-supervised learning dynamics without contrastive pairs. In *International Conference on Machine Learning*, pages 10268–10278. PMLR, 2021.
- [TYCG20] Yuandong Tian, Lantao Yu, Xinlei Chen, and Surya Ganguli. Understanding self-supervised learning with dual deep networks. *arXiv preprint arXiv:2010.00578*, 2020.
- [Ver10] Roman Vershynin. Introduction to the non-asymptotic analysis of random matrices. *arXiv preprint arXiv:1011.3027*, 2010.
- [ZJM⁺21] Jure Zbontar, Li Jing, Ishan Misra, Yann LeCun, and Stéphane Deny. Barlow twins: Self-supervised learning via redundancy reduction. *arXiv preprint arXiv:2103.03230*, 2021.
- [ZLR⁺23] Runtian Zhai, Bingbin Liu, Andrej Risteski, Zico Kolter, and Pradeep Ravikumar. Understanding augmentation-based self-supervised representation learning via rkhs approximation. *arXiv preprint arXiv:2306.00788*, 2023.

A Hilbert Space of functions

A.1 Functions and inner product space

Definition A.1. Given X, ρ_X , and $f, g : X \rightarrow \mathbb{R}$, define the $L^2(\rho_X)$ inner product and norm, respectively,

$$(f, g)_{\rho_X} = \int f(x)g(x)d\rho_X(x), \quad \|f\|_{\rho_X}^2 = (f, f)_{\rho_X} \quad (13)$$

Define

$$L^2(\rho, X) = \{f : X \rightarrow \mathbb{R} \mid \|f\|_{\rho_X}^2 < \infty\}$$

to be the (equivalence class) of functions with finite ρ_X norm.

A.2 Spectral theory

In this section we quote the relevant (abstract) Hilbert Space theory.

Definition A.2 (Spectral Operator). Given orthogonal functions, $\Phi = (\phi_i)_{i \in I}$ in $L^2(\rho_X)$, and non-negative $\Lambda = (\lambda_i)_{i \in I}$, with $\|\Lambda\|_2^2 = \sum_{i \in I} \lambda_i^2 < \infty$. Call (Φ, Λ) a spectral pair and define the corresponding spectral operator by

$$T_{\Phi, \Lambda}(h) = \sum_{j=1}^{\infty} \lambda_j (h, \phi_j) \phi_j, \quad (14)$$

Theorem A.3 (Spectral Decomposition). *Suppose H is a Hilbert space. A symmetric positive-definite Hilbert-Schmidt operator $T : \mathbb{H} \rightarrow \mathbb{H}$ admits the spectral decomposition equation 14 with orthonormal ϕ_j which are the eigenfunctions of T , i.e. $T(\phi_j) = \lambda_j \phi_j$. The ϕ_j can be extended to a basis by adding a complete orthonormal system in the orthogonal complement of the subspace spanned by the original ϕ_j .*

Remark A.4. The ϕ_j in equation 14 can thus be assumed to form a basis, but some λ_j may be zero.

From [HK12]. Theorem proved in [Goh90]. Denote by \mathcal{L} the space of bounded (continuous) linear operators on \mathbb{H} with the norm

$$\|T\|_{\mathcal{L}} = \sup\{\|T(x)\| \mid \|x\| \leq 1\}.$$

Definition A.5 (Compact Operators). An operator $T \in \mathcal{L}$ is said to be compact if there exist two orthonormal bases $\{g_j\}$ and $\{f_j\}$, and a real sequence $\{\lambda_j\}$ converging to zero, such that

$$T(h) = \sum_{j=1}^{\infty} \lambda_j (h, g_j) f_j, \quad h \in \mathbb{H}, \quad (\text{Compact})$$

The λ_j may be assumed positive. The existence of representation equation Compact is equivalent to the condition: T maps every bounded set into a compact set. Compact operators are also called completely continuous operators. Representation equation Compact is called the singular value decomposition.

Definition A.6 (Hilbert-Schmidt Operators). A compact operator admitting representation equation Compact is said to be a Hilbert-Schmidt operator if $\sum_{j=1}^{\infty} \lambda_j^2 < \infty$. The space \mathcal{S} of Hilbert-Schmidt operators is a separable Hilbert space with the scalar product

$$\langle T_1, T_2 \rangle_{\mathcal{S}} = \sum_{i=1}^{\infty} (T_1(f_i), T_2(f_i)), \quad (15)$$

where $\{f_i\}$ is an arbitrary orthonormal basis. Note the value of equation 15 is independent of the basis. The corresponding norm is

$$\|T\|_{\mathcal{S}}^2 = \sum_{j \geq 1} \lambda_j^2 \quad (\text{HS})$$

One can show that

$$\|T\|_{\mathcal{L}} \leq \|T\|_{\mathcal{S}}$$

Definition A.7. An operator $T \in \mathcal{L}$ is said to be symmetric if

$$\langle T(f), g \rangle = \langle f, T(g) \rangle, \quad f, g \in \mathbb{H},$$

and positive-definite if

$$\langle T(f), f \rangle \geq 0, \quad f \in \mathbb{H}.$$

(An operator with the last property is sometimes called positive semidefinite, and the term positive-definite is used when the inequality is strict.)

B Data augmentation kernel perspective of non-contrastive SSL

Theorem B.1. Let $G(x)$ be the infinite Mercer features of the backward data augmentation covariance kernels, k^{DAB} . Let $F(x) = (f_1(x), f_2(x), \dots, f_k(x))$ be the features given by minimizing the following data augmentation invariance loss

$$L(F) = \sum_{i=1}^{N_k} \|T_M f_i - f_i\|_{L^2(\rho_X)}^2, \quad \text{subject to} \quad (f_i, f_j)_{\rho_X} = \delta_{ij} \quad (16)$$

which includes the orthogonality constraint. Then, $V(F) \subset V(G)$, $V(F) \rightarrow V(G)$ as $N_k \rightarrow \infty$.

The idea of the proof uses the fact that, as linear operators, $T_{k^{DAB}} = T_M^\top T_M$ and that $T_{k^{DAF}} = T_M T_M^\top$. Then we use spectral theory of compact operators, which is analogue of the Singular Value Decomposition in Hilbert Space, to show that eigenfunctions of $T_M^\top T_M$ operator are the same as those obtained from optimizing $L(F)$. A similar result can be obtained using k^{DAF} and T_M^\top .

Note that $L(F)$ is the constrained optimization formulation of the BarlowTwins loss. Furthermore, $L(F)$ with the additional constraint that $(f_i, f_i) \geq \gamma \forall i \in \{1, 2 \dots N_k\}$ is the constrained optimization formulation of the VICReg loss.

B.1 Proof of theorem 3.2

We show we can factor the linear operator, leading to a practical algorithm. Here, we show that we can capture the backward data augmentation kernel with the forward data augmentation averaging operator

Lemma B.2. Using the definitions above, and with k in equation 8 given by k^{DAB} ,

$$T_k = T_M^\top T_M$$

Proof. First, define the non-negative definite bilinear form

$$B^{VAR}(f, g) = (T_M f, T_M g)_{\rho_X} \quad (17)$$

Given the backwards data augmentation covariance kernel, k^{DAB} , define

$$B^{DAB}(f, g) = (T_k f, g)_{\rho_X}$$

We claim, that

$$B^{VAR} = B^{DA,B} \quad (18)$$

This follows from the following calculation,

$$B^{DA,B}(f, g) = (T_k f, g)_{\rho_X} \quad (19)$$

$$= \mathbb{E}_x [T_k f(x), g(x)] = \mathbb{E}_x \mathbb{E}_z [k_{DA,B}(z, x) f(z) g(x)] \quad (20)$$

$$= \mathbb{E}_x \mathbb{E}_z \mathbb{E}_{x_0} [p(x | x_0) p(z | x_0) f(z) g(x)] \quad (21)$$

$$= \mathbb{E}_{x_0} [\mathbb{E}_x [p(x | x_0) g(x)], \mathbb{E}_z [p(z | x_0) f(z)],] = \mathbb{E}_{x_0} T_M f(x_0) T_M g(x_0) \quad (22)$$

$$= (T_M f, T_M g)_{\rho_X} = B^{VAR}(f, g) \quad (23)$$

□

For implementations, it is more natural to consider *invariance* to data augmentations.

Theorem B.3 (equivalent eigenfunctions). *Assume that T_M is a compact operator. Define the invariance bilinear form*

$$B^{INV}(f, g) = (T_M f - f, T_M g - g) \quad (24)$$

Then B^{INV} , B^{VAR} share the same set of eigenfunctions. Moreover, these are the same as the eigenfunctions of $B^{DA,B}$. In particular, for any eigenfunction f_j of B^{VAR} , with eigenvalue λ_j , then f_j is also an eigenfunction of B^{INV} , with the corresponding eigenvalue given by $(\sqrt{\lambda_j} - 1)^2$.

Proof. Define T_{MM} by,

$$T_{MM} f = T_M^\top T_M f \quad (25)$$

Define

$$T_{MS} = (T_M - I)^\top (T_M - I) \quad (26)$$

Note, by the assumption of compactness, T_M has the Singular Value Decomposition, (see the Hilbert Space section for equation [SVD](#)),

$$T_M(h) = \sum_{j=1}^{\infty} \lambda_j(h, g_j) f_j \quad (\text{SVD})$$

Let f_j be any right eigenvector of T_M , with eigenvalue μ_j . Then f_j is also a right eigenvector of $T_M - I$, with eigenvalue $\mu_j - 1$. So we see that T_{MM} has f_j as an eigenvector, with eigenvalue $\lambda_j = \mu_j^2$ and T_{MS} has f_j as an eigenvector, with eigenvalue $(\sqrt{\lambda_j} - 1)^2$. Finally, the fact that there are no other eigenfunctions also follows from equation [SVD](#).

The final part follows from the previous lemma. □

C Multi-Augmentation Learning

C.1 Augmentation graph

We use the population augmentation graph formulation introduced in [[HWGM21](#)]. Briefly, we define a graph $\mathcal{G}(\mathcal{X}, \mathcal{W})$, where the vertex set \mathcal{X} comprises of all augmentations from the dataset (could be infinite when continuous augmentation functions are used) and \mathcal{W} denotes the adjacency matrix with edge weights as defined below:

$$w_{xx'} := \mathbb{E}_{\bar{x} \sim \mathcal{P}_{\bar{x}}} [\mathcal{A}(x|\bar{x}) \mathcal{A}(x'|\bar{x})] \quad (27)$$

, i.e. the joint probability of generating ‘patches’ x, x' from the same image \bar{x} . Here \mathcal{A} defines the set of augmentation functions used in the SSL pipeline. It is worth noting that the magnitude of $w_{xx'}$

captures the relative similarity between x and x' . A higher value of $w_{xx'}$ indicates that it is more likely that both patches came from the same image, and thereby are more similar. The marginal likelihood of each patch x can also be derived from this formulation:

$$w_x = \mathbb{E}_{x' \sim \mathcal{X}} [w_{xx'}] \quad (28)$$

C.2 Contrastive and non-contrastive losses suffer from the same issues

We will now show that using multiple patches for the $\mathcal{L}_{invariance}$ is pertinent to both the contrastive and non-contrastive SSL. Following [HWGM21], we use the spectral contrastive loss formulation and incorporate the augmentation graph relations:

$$\begin{aligned} \mathcal{L}_c &= -\mathbb{E}_{x, x^+} [f(x)^T f(x^+)] + \beta \mathbb{E}_{x, x'} [(f(x)^T f(x'))^2] \\ \mathcal{L}_c &\propto \|ZZ^T - D^{-\frac{1}{2}} \mathcal{W} D^{-\frac{1}{2}}\|_F^2 = \|ZZ^T - \bar{\mathcal{W}}\|_F^2 \end{aligned} \quad (29)$$

where $z := \sqrt{w_x} f(x)$, D is a $N \times N$ diagonal matrix with entries $\{w_x\}$ and $\bar{\mathcal{W}} = D^{-\frac{1}{2}} \mathcal{W} D^{-\frac{1}{2}}$.

We extend the duality results between contrastive and non-contrastive SSL loss, established by [GCB⁺22], to demonstrate how eq. (29) can be decomposed into the invariance and collapse-preventing loss terms.

$$\|ZZ^T - \bar{\mathcal{W}}\|_F^2 = \|Z^T Z - I_d\|_F^2 + 2\text{Tr} [Z^T (I_N - \bar{\mathcal{W}}) Z] + \kappa \quad (30)$$

$$= \|Z^T Z - I_d\|_F^2 + 2 \sum_i \sum_x (1 - \bar{w}_x) z_i^2 - 2 \sum_i \sum_{x, x'} \bar{w}_{xx'} z_i z'_i + \kappa \quad (31)$$

where κ is some constant independent of Z . The first term in eq. (30) is the covariance regularization term in non-contrastive losses like BarlowTwins (implicit) or VIC-Reg (explicit), and the second term in eq. (31) is the variance regularization. Simplifying the third term in eq. (31) gives us:

$$\begin{aligned} \sum_i \sum_{x, x'} \bar{w}_{xx'} z_i z'_i &= \sum_i \sum_{x, x'} w_{xx'} f(x)_i f(x')_i = \sum_i \sum_{x, x'} \mathbb{E}_{\bar{x} \sim \mathcal{P}_{\bar{x}}} [\mathcal{A}(x|\bar{x}) \mathcal{A}(x'|\bar{x}) f(x)_i f(x')_i] \\ &= \sum_i \mathbb{E}_{\bar{x} \sim \mathcal{P}_{\bar{x}}} \left[\sum_x \mathcal{A}(x|\bar{x}) (f(x)_i \overline{f(x)_i} - f(x)_i^2) \right] \\ &= \mathbb{E}_{\bar{x} \sim \mathcal{P}_{\bar{x}}} \left[\sum_x \mathcal{A}(x|\bar{x}) \left(f(x)^T \overline{f(x)} - \|f(x)\|^2 \right) \right] \end{aligned} \quad (32)$$

This term encourages $f(x)$ to be similar to $\overline{f(x)}$, i.e. the mean representation across all augmentations of \bar{x} , thereby requiring to “sufficiently” sample $A(\cdot|\bar{x})$. Given that both the contrastive and non-contrastive losses rely on learning invariance properties from data augmentations, we believe that our multi-patch proposal would improve the probability density estimation of $A(\cdot|\bar{x})$ and yield better performance with few training epochs.

C.3 Explaining training dynamics in low patch sampling regime

We now turn to a simple form of the augmentation graph to understand how using low number of augmentations affects the evolution of ZZ^T . Minimizing eq. (29) implies that the spectral decomposition of Z would align with the top eigenvectors (and values) of $\bar{\mathcal{W}}$. We will demonstrate that in the low sampling regime (using few augmentations), the eigenvectors of the sampled augmentation graph $\tilde{\mathcal{W}}$ may not align with those of $\bar{\mathcal{W}}$.

Augmentation graph setup. We define an augmentation graph with only two instances from two different classes, similar to the one presented in [SJK⁺22]. Let us denote the four instances as \bar{x}_i for $i \in 1, 2, 3, 4$, where \bar{x}_1, \bar{x}_2 belong to class 1 (i.e. $y_1, y_2 = 1$) and \bar{x}_3, \bar{x}_4 belong to class 2 (i.e. $y_3, y_4 = 4$). Let us further assume that \bar{x}_1, \bar{x}_3 have the highest pixel-level similarity among $(\bar{x}_1, \bar{x}_i) \forall i \in 2, 3, 4$, thereby making it more likely to have similar patches (see Figure 2 for illustration). We denote this relationship among input examples using \mathcal{G} to indicate (pixel-wise) global similarity groups. So, $\mathcal{G}_1, \mathcal{G}_3 = 1$ and $\mathcal{G}_2, \mathcal{G}_4 = 2$. We can use the following probabilistic formulation to model our augmentation functions (see Figure 2B):

$$A(x_j|\bar{x}_i) = \begin{cases} \rho' & \text{if } j = i \\ \mu' & \text{if } j \neq i \text{ and } y_j = y_i \text{ and } \mathcal{G}_j \neq \mathcal{G}_i \\ \nu' & \text{if } j \neq i \text{ and } y_j \neq y_i \text{ and } \mathcal{G}_j = \mathcal{G}_i \\ \delta' & \text{if } j \neq i \text{ and } y_j \neq y_i \text{ and } \mathcal{G}_j \neq \mathcal{G}_i \end{cases} \quad (33)$$

In our setting, $\rho' + \mu' + \nu' + \delta' = 1$. The adjacency matrix of our augmentation graph (as shown in Figure 2C) is as follows:

$$\overline{\mathcal{W}} = \begin{bmatrix} \rho & \mu & \nu & \delta \\ \mu & \rho & \delta & \nu \\ \nu & \delta & \rho & \mu \\ \delta & \nu & \mu & \rho \end{bmatrix} \quad (34)$$

We defer the relations between $\rho', \mu', \nu', \delta'$ and ρ, μ, ν, δ to the appendix. The eigenvalues of this matrix are: $(\rho + \mu + \nu + \delta, \rho + \mu - \nu - \delta, \rho - \mu + \nu - \delta, \rho - \mu - \nu + \delta)$. Corresponding eigenvectors are along $[1, 1, 1, 1]^T, [1, 1, -1, -1]^T, [1, -1, 1, -1]^T, [1, -1, -1, 1]^T$. Assuming that the augmentation functions induce semantically-relevant invariance properties that are relevant for identifying y_i from $f(x_i)$, we can say that $\rho' > \max\{\mu', \nu'\}$ and $\min\{\nu', \mu'\} > \delta'$. When we have sufficiently sampled the augmentations, any SSL loss will learn Z such that its singular values are span the top eigenvectors of the augmentation graph, and the eigenspectrum of ZZ^T would simply be the above eigenvalues. In practical settings, the augmentation graph would have significantly higher dimension than the feature/embedding dimension¹. Therefore, singular vectors of Z would span the top eigenvectors of $\overline{\mathcal{W}}$ and the smaller eigenmodes are not learned. When we have accurately sampled the augmentation graph, $\mu > \nu$ and therefore, the class-information preserving information is preferred over pixel-level preserving information during learning. But what happens when we *do not sufficiently sample the augmentation space*?

Ansatz. Based on our empirical experience, we define *an ansatz* pertaining to the eigenvalues of a sampled augmentation graph and validate it in tractable toy settings, such as the one described above. Specifically, we claim that when the augmentation space is not sufficiently sampled, $\{|\mu - \nu|, \delta\} \rightarrow 0$. In other words, we claim that when only few augmentations per example are used, it is more likely to have an equal empirical likelihood for augmentations that preserve (pixel-level) global information and class/context information. Moreover, it is very unlikely to have augmentations that change both the class and global information. This is demonstrated in Figure 7.

Consequences of the Ansatz. When only a few augmentations are sampled, learning can suppress the class information at the cost of preserving the pixel-level information, thereby leading to an increased smoothness in the learned feature space.

¹Contrastive algorithms use a large batch size, thereby optimizing a high-dimensional ZZ^T whereas non-contrastive algorithms use a large embedding dimension, thereby optimizing a high-dimensional $Z^T Z$.

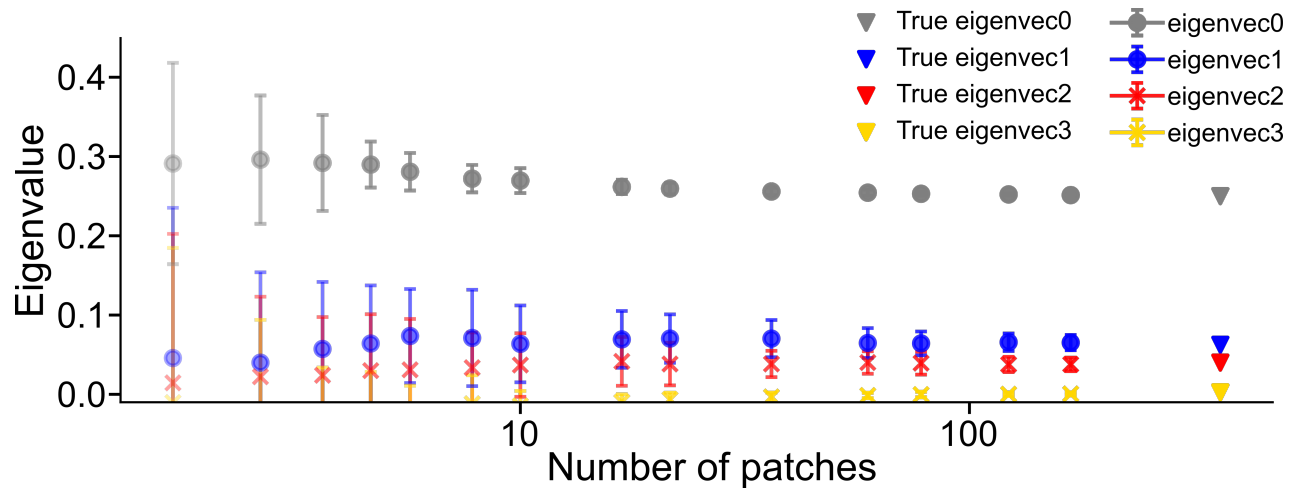


Figure 7: Empirical verification of the subsampling Ansatz.

D Implementation Details

Image Classification Datasets Across all experiments, our settings mainly follow [CBLL22]. In particular, we run Table 1a summarizes our pretraining settings on Cifar-10 [KH09], and STL-10 [CNL11]. In Table 1b, we outline the corresponding linear evaluation settings for Resnet-50. Note that we add a linear classifier layer to the encoder’s features and discard the projection layers for evaluation.

config	value	config	value
optimizer	Adam	optimizer	Adam
learning rate	1e-3	learning rate	1e-3
batch size	128	batch size	512
epochs	100 (CIFAR10), 50 (STL10)	epochs	200
weight-decay	1e-6	weight-decay	1e-6
		test-patches	16

(a) Pretraining

(b) Linear Evaluation

Table 1: Experiment Protocol for comparing SSL algorithms

D.1 Longer Pretraining

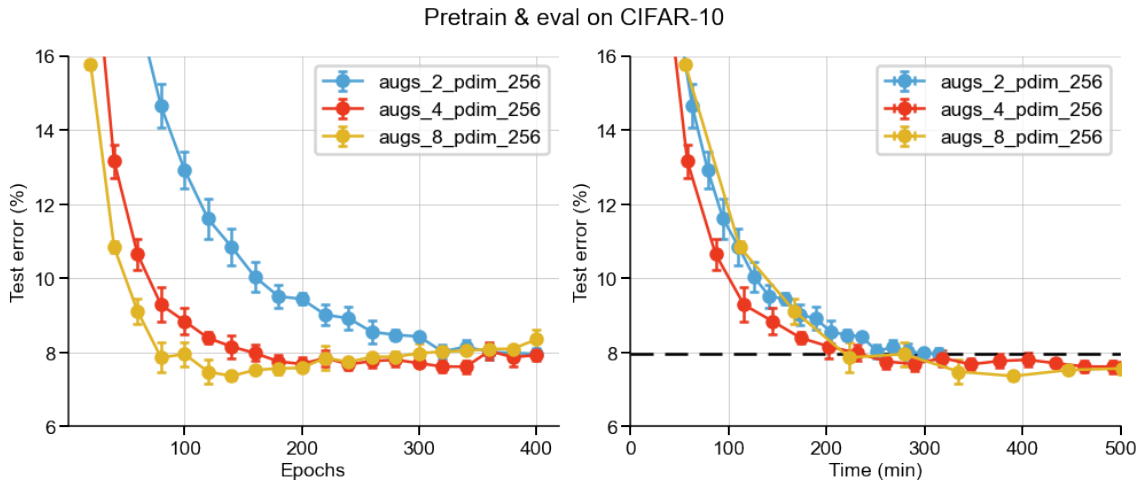


Figure 8: BarlowTwins pretraining on full CIFAR-10 dataset for 400 epochs.

Algorithm	Best accuracy	Best accuracy @ epoch
Barlow-Twins (2-augs) w/ pdim=256	92.04 +/- 0.16	400
Barlow-Twins (4-augs) w/ pdim=256	92.39 +/- 0.17	340
Barlow-Twins (8-augs) w/ pdim=256	92.64 +/- 0.10	140

Table 2: BarlowTwins pretraining on full CIFAR-10 dataset at 400 epochs (with early stopping)

D.2 SwAV-like augmentations for compute efficient multi-augmentation framework

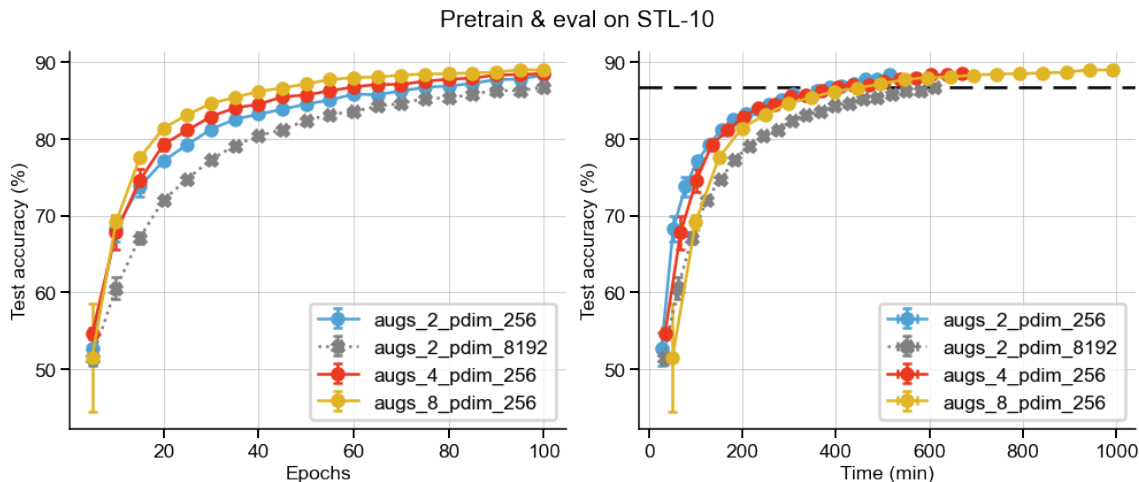


Figure 9: BarlowTwins pretraining on full STL-10 dataset for 100 epochs using SwAV-like augmentations. Specifically, the 2-augmentations setting uses two views that are 64×64 , whereas the 4 (or 8) augmentation setting uses additional two (or six) augmentations that are 32×32 .

D.3 On training with full dataset with 4/8 augmentations

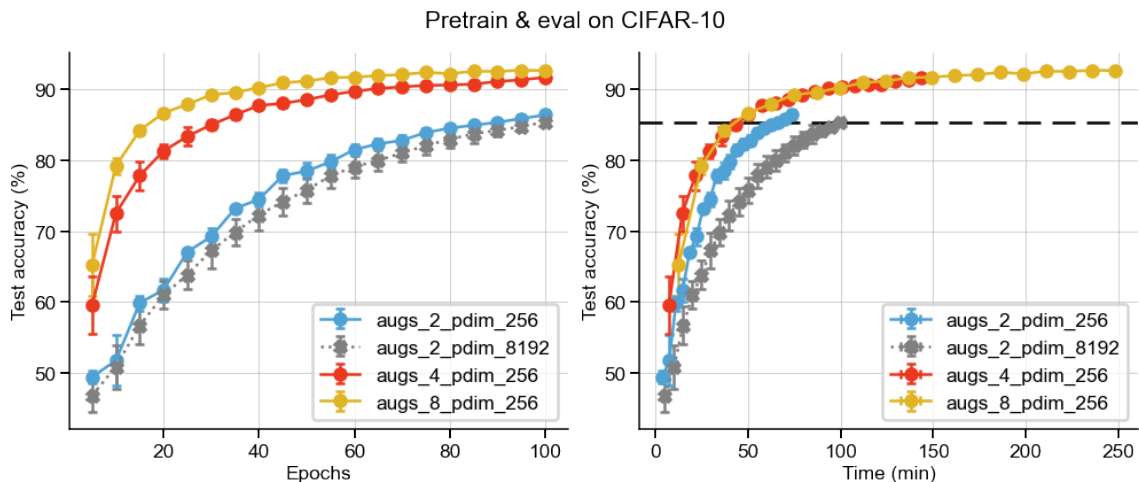


Figure 10: BarlowTwins pretraining on full CIFAR-10 dataset.

Algorithm	#augs=2	#augs=4	#augs=8
Barlow-Twins w/ pdim=256	86.43 +/- 0.72	91.73 +/- 0.16	92.71 +/- 0.19
Barlow-Twins w/ pdim=8192	85.44 +/- 0.54	91.40 +/- 0.32	92.40 +/- 0.13

Table 3: BarlowTwins pretraining on full CIFAR-10 dataset at 100 epochs

D.4 Empirical results on transfer learning

In this section, we present extended version of results presented in Figure 4, Figure 5 but pretraining on CIFAR-10 (or STL-10) and evaluating on STL-10 (or CIFAR-10). These results, coupled with the ones in Figure 4 Figure 5, present a strong case for the advantage of using the proposed multi-augmentation loss for better convergence as well as downstream accuracy.

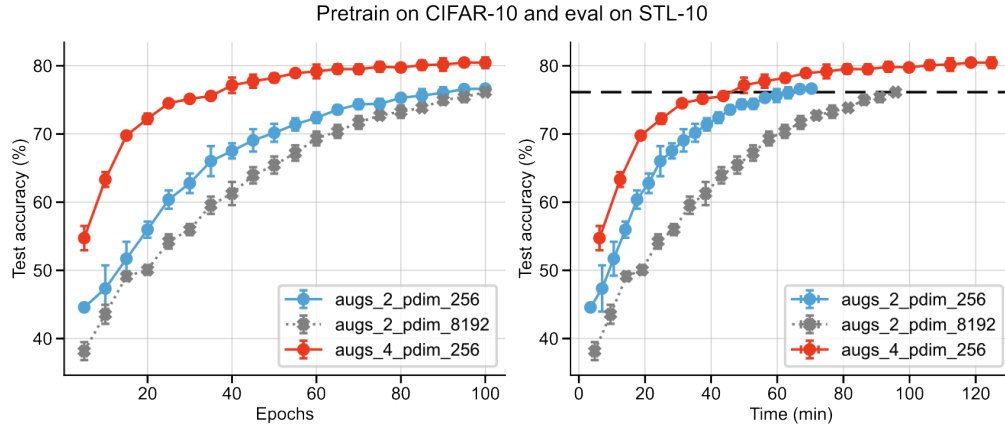


Figure 11: BarlowTwins pretraining on CIFAR-10, linear evaluation on STL-10 labelled set.

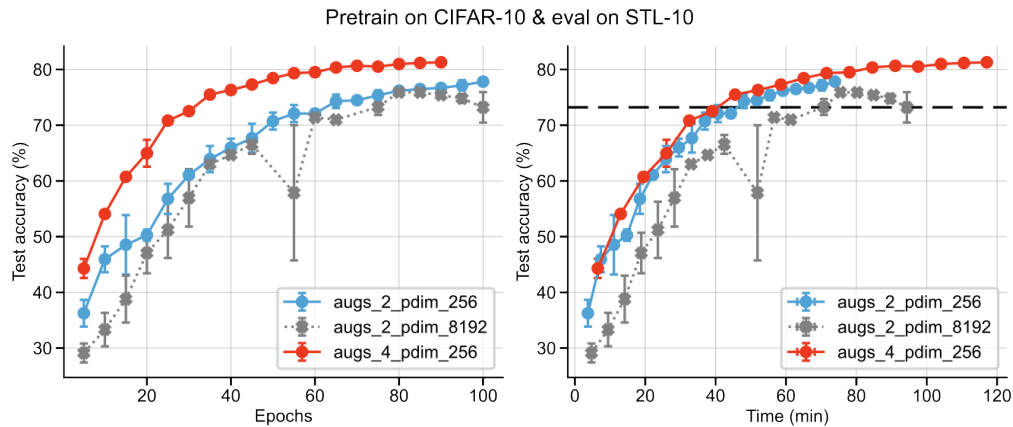


Figure 12: VICReg pretraining on CIFAR-10, linear evaluation on STL-10 labelled set.

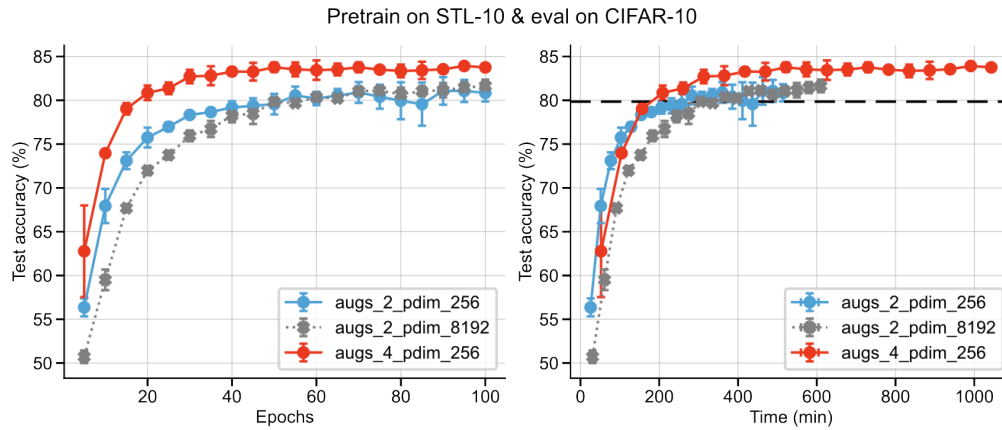


Figure 13: BarlowTwins pretraining on STL-10, linear evaluation on CIFAR-10 labelled set.

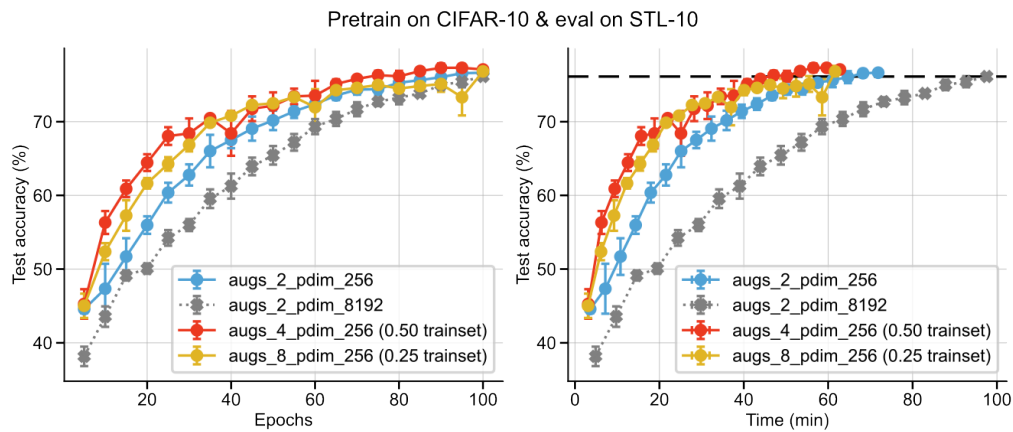


Figure 14: BarlowTwins pretraining on fraction of CIFAR-10 trainset, linear evaluation on STL-10 labelled set.

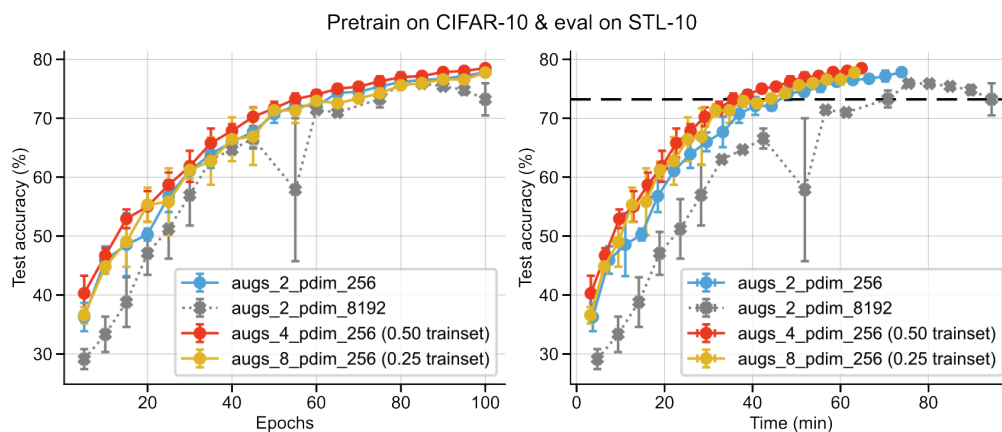


Figure 15: VICReg loss pretraining on fraction of CIFAR-10 trainset, linear evaluation on STL-10 labelled set.

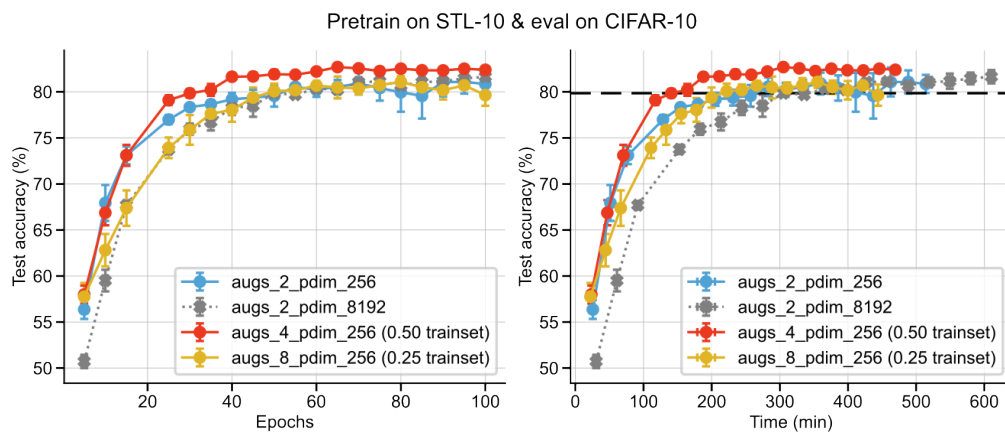


Figure 16: BarlowTwins loss pretraining on fraction of STL-10 unlabelled set, linear evaluation on CIFAR-10 train set.